INDIAN JOURNAL OF SCIENCE AND TECHNOLOGY

ORIGINAL ARTICLE

Check for updates

OPEN ACCESS

**Received:** 30/07/2026

**Accepted:** 30/09/2026

**Published:** 22/10/2026

**Citation:** Rajitha N, Srinivasan V, Sathishkumar GB (2026) Comparative Study on Wear Behavior, Corrosion Resistance, and Bioactivity Performance of Conventional and nTopology-Designed DMLS Co-Cr Alloys for Biomedical Implant Applications. Indian Journal of Science and Technology 19(37): 2601-2611. https://doi.org/10.17485/IJST/v19i37.1120

* **Corresponding author**.

narerajitha.phd@gmail.com

**Funding:** None

**Competing Interests:** None

**Copyright:** © 2026 Rajitha et al. This is an open access article distributed under the terms of the Creative Commons Attribution License, which permits unrestricted use, distribution, and reproduction in any medium, provided the original author and source are credited.

Published By Indian Society for Education and Environment (iSee)

**ISSN**
Print: 0974-6846
Electronic: 0974-5645

# Comparative Study on Wear Behavior, Corrosion Resistance, and Bioactivity Performance of Conventional and nTopology-Designed DMLS Co-Cr Alloys for Biomedical Implant Applications

**N Rajitha[1]*, V Srinivasan[1], G B Sathishkumar[2]**

**1** Department of Manufacturing Engineering, Faculty of Engineering and Technology, Annamalai University, Annamalai Nagar, Chidambaram, 608002, Tamil Nadu, India
**2** Department of Mechanical Engineering, Arasu Engineering College, Chennai Main Road, Kumbakonam, 608002, Tamil Nadu

## Abstract

**Objectives:** To make a comparative study on the wear behavior, corrosion resistance, and bioactivity performance of conventional Co-Cr (Cobalt-Chromium) alloy and nTopology-designed Co-Cr alloy sintered by Direct Metal Laser for biomedical implant applications. **Method: C**omparative investigations were made on the CM-CoCr (Conventional Co-Cr) alloy and NT-DMLS-CoCr (nTopology-designed DMLS Co-Cr) alloy specimens. By using pin-on-disc tribometer wear tests were performed under 10, 30, and 50 N loads at a sliding velocity and a sliding distance of 1.25 m/s and 1000 m respectively. Corrosion behavior was also evaluated with the help of potentiodynamic polarization test in simulated body fluid (SBF) at 37°C. Bioactivity behavior was assessed by immersing the specimens in SBF for a duration of up to 28 days and monitoring the apatite formation. Here CM-CoCr was chosen as the control material for comparison. **Findings:** The NT-DMLS-CoCr specimens exhibited better tribological, electrochemical, and bioactive performance when compared with CM-CoCr. At 50 N, the wear rate decreased from $6.24 \times 10^{-5}$ $mm^3$/Nm for CM-CoCr to $3.46 \times 10^{-5}$ $mm^3$/Nm for NT-DMLS-CoCr, representing a reduction of approximately 44.5%. The friction coefficient also gets decreased from 0.55 to 0.43. Potentiodynamic polarization studies concluded that the corrosion current density gets decreased from 1.76 $\mu A/cm^2$ to 0.42 $\mu A/cm^2$, while the corrosion rate gets reduced from 0.017 mm/year to 0.004 mm/year. Bioactivity evaluation revealed enhanced apatite formation, with NT-DMLS-CoCr achieving apatite coverage of 95% after 28 days compared to that of 68% for CM-CoCr. The enhanced performance is attributed in the refined DMLS microstructure and interconnected gyroid lattice architecture, which improved load distribution, passive film stability, and biomineralization behavior. **Novelty:** This study presents a comparative evaluation of conventional and nTopology-designed DMLS Co-Cr alloys, exhibiting the advantages of lattice-engineered additive manufacturing best suited for biomedical implant applications.

**Keywords:** Co-Cr; nTopology; DMLS; Biomedical applications

## 1 Introduction

Biomedical implants are subjected to mechanical loading, frictional contact, physiological fluids, and biological interactions throughout their service life. Therefore, implant materials require an appropriate combination of mechanical strength, wear resistance, corrosion resistance, and biological compatibility [1]. Cobalt–chromium (Co-Cr) alloys are widely used in orthopedic and dental applications because of their high strength, hardness, wear resistance, and corrosion resistance [2], [3]. However, implant performance depends not only on alloy composition but also on the manufacturing process, surface characteristics, and internal architecture.

Conventional Co–Cr implants are commonly manufactured through casting, forging, and machining. Although these processes provide established manufacturing routes, they have limitations in producing complex internal geometries, interconnected porous structures, and patient-specific architectures. Machining can also result in material wastage, while conventional processing generally produces dense structures with limited control over porosity and pore interconnectivity [4], [5]. These limitations may restrict bone-mimicking architectural design and contribute to stress shielding and reduced biological fixation. Consequently, advanced manufacturing approaches are required to provide greater geometric freedom and improved control over implant architecture [6].

Direct Metal Laser Sintering (DMLS) provides greater freedom for fabricating complex metallic structures directly from digital models and can produce geometries that are difficult to manufacture using conventional techniques [7], [8], [9], [10]. However, DMLS performance remains dependent on processing parameters, thermal history, powder characteristics, surface condition, and manufacturing-related defects. Furthermore, DMLS alone does not determine the optimal internal architecture of an implant. Computational design platforms such as nTopology can complement DMLS by enabling controlled generation of lattice structures with defined topology, porosity, unit-cell dimensions, and material distribution [11]. Nevertheless, lattice design involves a balance between porosity, structural integrity, material utilization, and biological functionality. Therefore, appropriate architectural design is essential for obtaining a suitable implant structure.

In the present study, a gyroid lattice architecture was designed using nTopology and fabricated using DMLS with a relative density of 40%, porosity of 60%, and unit-cell size of 600 $\mu$m. The interconnected architecture was selected to provide controlled material distribution and an open internal structure while maintaining a defined structural framework. The combined nTopology–DMLS approach is intended to overcome the geometric and architectural limitations of conventional Co–Cr manufacturing and provide greater control over the characteristics of the implant structure.

Despite increasing research on DMLS and computational lattice structures, limited studies have directly compared conventionally manufactured Co–Cr with nTopology-designed DMLS Co–Cr using an integrated assessment of wear, electrochemical corrosion, and bioactivity. Most existing investigations have focused on individual properties such as mechanical behavior, microstructure, corrosion, or biological response. Therefore, the combined influence of lattice architecture and DMLS fabrication on tribological, electrochemical, and bioactive performance remains insufficiently established.

The novelty of the present study lies in the direct experimental comparison of CM-CoCr and NT-DMLS-CoCr using a common evaluation framework. Wear behavior was investigated under applied loads of 10, 30, and 50 N at a sliding velocity of 1.25 m/s and a sliding distance of 1000 m. Electrochemical behavior was evaluated using potentiodynamic polarization in simulated body fluid, while bioactivity was assessed through apatite formation after 7, 14, 21, and 28 days of SBF immersion. Thus, the study aims to determine whether integrating computational gyroid lattice design with DMLS fabrication provides measurable advantages over conventional Co–Cr manufacturing for biomedical implant applications.

## 2 Methodology

The present study employed a comparative experimental methodology to evaluate the tribological, electrochemical, and bioactive performance of CM-CoCr and NT-DMLS-CoCr. CM-CoCr was considered the conventional reference/control material, whereas NT-DMLS-CoCr represented the proposed combination of computational lattice design and additive manufacturing. The methodology was strengthened by maintaining controlled fabrication and testing conditions, defining the lattice architecture and its selection criteria, using repeated measurements, and applying quantitative comparison between the two material groups. The experimental workflow consisted of material preparation, DMLS fabrication, nTopology-based lattice design, wear testing, potentiodynamic polarization testing, and SBF-based bioactivity evaluation.

### 2.1 Materials

Two Co–Cr alloy material groups were investigated: CM-CoCr and NT-DMLS-CoCr. The CM-CoCr specimens were manufactured through conventional casting and machining processes and were used as the reference material. The NT-DMLS-

CoCr specimens were fabricated from gas-atomized Co–Cr alloy powder using a DMLS system after incorporating a lattice architecture generated using nTopology software. The use of CM-CoCr as the control enabled direct quantitative comparison of the effects associated with the DMLS fabrication route and computationally designed internal architecture.

#### *2.1.1. Conventional Co-Cr Alloy (CM-CoCr)*

Commercially available conventionally manufactured Co–Cr alloy specimens were selected as the reference/control material. The specimens were produced using conventional casting followed by machining and were prepared according to the dimensions required for the respective wear, electrochemical, and bioactivity experiments. Conventional Co–Cr alloys are established biomaterials because of their high strength, hardness, wear resistance, and corrosion resistance. However, their predominantly dense architecture and restricted geometric flexibility limit the fabrication of interconnected porous structures and complex internal geometries. In the present investigation, CM-CoCr was used as the conventional benchmark against which the performance of the nTopology-designed DMLS specimens was quantitatively assessed.

#### *2.1.2. Co–Cr Alloy Powder for NT-DMLS-CoCr*

Gas-atomized Co–Cr alloy powder specifically intended for DMLS fabrication was used to manufacture the NT-DMLS-CoCr specimens. The powder particle-size distribution was 15–45 $\mu$m. The powder composition consisted primarily of cobalt and chromium, with molybdenum and minor alloying elements including silicon, manganese, and iron. The chemical composition of the Co–Cr powder is presented in Table 1.

**Table 1.** Chemical Composition of Co-Cr Alloy Powder (wt.%)

| Element | Co | Cr | Mo | Si | Fe | Mn | Ni | W | C |
|---|---|---|---|---|---|---|---|---|---|
| Content | 60-65 | 27-30 | 5-7 | 1-2 | 0.5-1 | 0.5-1 | <0.1 | <0.1 | <0.1 |

The relatively high chromium content provides the alloy with corrosion resistance through the development of a protective passive surface film, while molybdenum contributes to alloy strength and resistance to localized corrosion. The controlled particle-size range and spherical morphology of gas-atomized powder are suitable for consistent powder spreading and layer formation during DMLS processing. The same powder composition and fabrication conditions were maintained for the NT-DMLS-CoCr specimens to minimize material-related variation during comparative testing.

The morphology of the Co-Cr powder was analyzed by using Scanning Electron Microscopy (SEM), as depicted in Figure 1(a). The particles experienced a predominantly spherical shape with a uniform size distribution, resulting excellent powder packing and flow characteristic parameters during DMLS processing.

Energy Dispersive X-ray Spectroscopy (EDS) study was carried out to examine the chemical composition of the powder, as given in Figure 1(b). The spectrum concluded the presence of cobalt (Co), chromium (Cr), and molybdenum (Mo) as the major alloying elements. Strong peaks corresponding to Co and Cr show that these elements hold the major portion of the alloy, while Mo is in lesser proportions. The observed composition fulfils the material requirements for biomedical implant applications requiring high corrosion resistance and mechanical strength.

## 2.2 Direct Metal Laser Sintering (DMLS) Fabrication

The NT-DMLS-CoCr specimens were manufactured by using an EOS M290 Direct Metal Laser Sintering apparatus fitted with a Yb-fiber laser. DMLS is a powder-bed fusion additive manufacturing process where the successive layers of metal powder are individually melted by using a high-energy laser beam to manufacture 3D components directly from digital models.

The DMLS system contains a build chamber, powder supply system, gas control unit, recoater mechanism, and process monitoring system, as shown in Figure 2(a). An inert argon atmosphere was maintained throughout the manufacturing process to reduce oxidation and ensure metallurgical integrity.

During production, a thin layer of Co-Cr powder was spread evenly over the build platform by a recoater blade. The laser beam directed through an X–Y scanning system and focusing optics, locally melted the powder based on the sliced CAD geometry. Upon completion of every layer, the build platform was brought down to one layer thick and a new powder layer was deposited. This layer-by-layer process was repeated done until the entire component was produced, as schematically shown in Figure 2(b).

The DMLS parameters listed in Table 2 were maintained constant for all NT-DMLS-CoCr specimens to ensure consistent fabrication conditions. A laser power of 200 W, scan speed of 1200 mm/s, hatch spacing of 0.1 mm, and layer thickness of 30 $\mu$m were employed with an argon shielding atmosphere and a build-platform temperature of 200°C. These conditions were

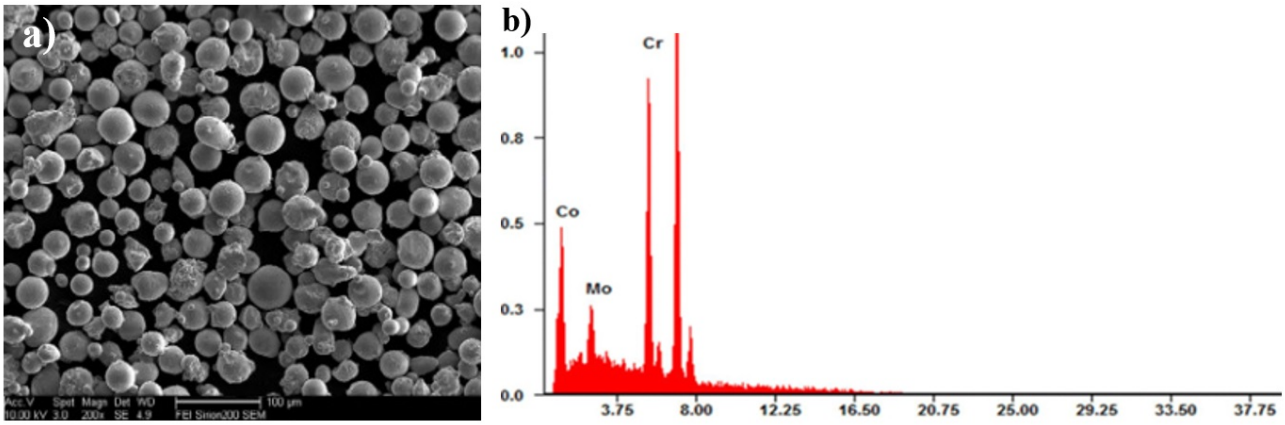



**Fig 1.** (a) SEM image of Co-Cr alloy powder (b) EDS spectrum of Co-Cr alloy powder

**Table 2.** DMLS Process Parameters

| Parameter | Value |
|---|---|
| Laser Power | 200 W |
| Layer Thickness | 30 $\mu$m |
| Speed of scan | 1200 mm/s |
| Shielding Gas | Argon |
| Hatch Spacing | 0.1 mm |
| Build Platform | Preheated to 200°C |

selected to obtain a high-density Co–Cr structure with controlled thermal conditions while minimizing oxidation and excessive thermal gradients during fabrication. Maintaining identical process parameters for all NT-DMLS-CoCr specimens ensured that subsequent differences in measured performance could be evaluated consistently.

The identified parameters were optimized to attain components with high-density, minimum porosity and refined microstructural characteristics. The preheated build platform lowered thermal gradients and residual stresses, while the presence of argon atmosphere prevented the oxidation during processing.

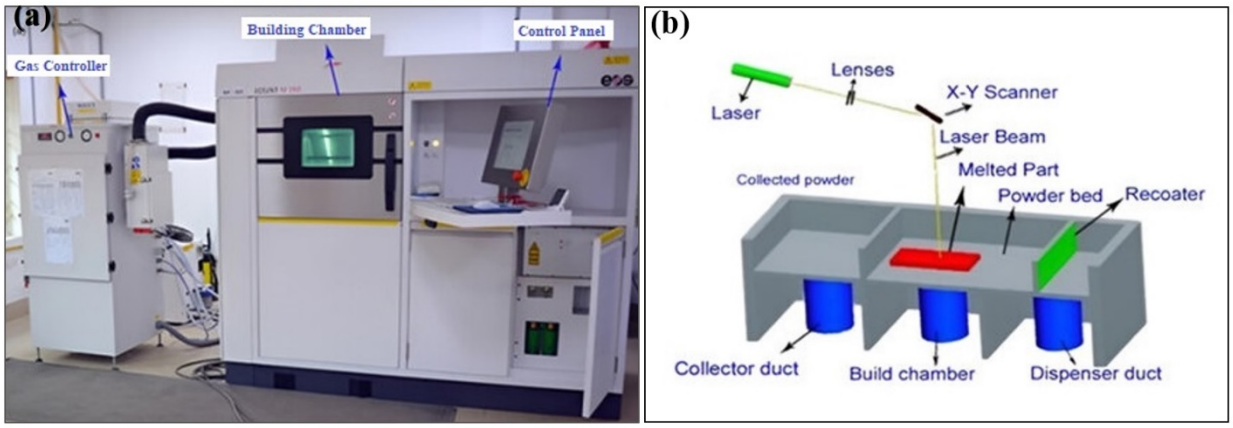



**Fig 2.** (a) Experimental setup of DMLS system (b) Schematic illustration of DMLS fabrication process

## 2.3 nTopology Design Integration

Advanced computer aided design software, nTopology, was used to produce lattice-based implant structures for the NT-DMLS-CoCr specimens. The aim of incorporating nTopology was to fabricate lightweight structures with improved mechanical characteristics and enhanced biological compatibility[12].

The design process initiated with importing the actual Computer-Aided Design (CAD) model into the nTopology environment. Subsequently, lattice structures were included within the specimen geometry to lower weight while maintaining required structural integrity. A gyroid lattice architecture was chosen owing to its better load sharing characteristics, interlinked porosity, and capability to facilitate the biological tissue ingrowth.

The optimized lattice design was done by adjusting the cell size, thickness of strut, and distribution of porosity. Functionally graded lattice regions were included to make sure even stress distribution while increasing stiffness in significant load-bearing situations. The optimized design held approximately 60% porosity with 600 $\mu$m unit cell size, giving a balance between biological performance and mechanical strength.

The inclusion of lattice structures notably increased the surface area available for hydroxyapatite nucleation and cellular attachment, which is expected to improve osseointegration. Furthermore, the interlinked pore network facilitates the nutrient transport and bone tissue infiltration, thereby encouraging long-term implant fixation.

After optimization, the completed nTopology design was exported in a compatible format with the EOS M290 DMLS system and then fabricated using the process parameters mentioned in Table 2. The nTopology lattice-design workflow consisted of CAD model import, lattice generation, geometric parameter selection, structural assessment, and preparation of the final design for DMLS fabrication. A gyroid lattice architecture was selected because of its continuous interconnected geometry, which provides a favorable balance between load distribution and open porosity. The lattice parameters were defined as a relative density of 40%, corresponding to 60% porosity, with a unit-cell size of 600 $\mu$m. These parameters were selected to reduce material usage while maintaining an interconnected architecture suitable for load transfer and biological interaction. The resulting lattice geometry was incorporated into the specimen model and converted into a DMLS-compatible file for fabrication. The selected lattice configuration and its corresponding parameters are summarized in Table 3.

**Table 3.** Characteristics of NT-DMLS-CoCr Lattice Structure

| Parameter | Value |
|---|---|
| Lattice Type | Gyroid |
| Relative Density | 40% |
| Porosity | 60% |
| Unit Cell Size | 600 $\mu$m |
| Fabrication Method | DMLS |
| Design Platform | nTopology |

The fabricated CM-CoCr and NT-DMLS-CoCr specimens were then subjected to wear testing, potentiodynamic polarization analysis, and bioactivity assessment to comparatively evaluate their adaptability for the applications in biomedical implants.

## 2.4 Wear Behavior Evaluation

The wear characteristics of CM-CoCr alloy and NT-DMLS-CoCr alloy specimens were examined by using a pin-on-disc apparatus as per the ASTM G99 standards[13]. Before testing, by using silicon carbide abrasive papers the specimens were polished, cleaned ultrasonically in ethanol, and dried to make sure an even surface condition. With the help of an alumina counterface disc wear tests were done under dry sliding conditions[14]. To evaluate the impact of applied load on tribological performance, three different loads of 10 N, 30 N and 50 N were applied, at a constant sliding velocity of 1.25 m/s and a sliding distance of 1000 m for all experiments. The coefficient of friction (CoF) was regularly observed during testing, and the wear rate was evaluated from the material loss at the end of each test. To ensure correctness of the observations, all experiments were repeated three times and the average values were recorded. After the wear test, the worn surfaces were analyzed by using SEM to identify the dominant wear mechanisms and compare the tribological performance of CM-CoCr and NT-DMLS-CoCr specimens[15].

### 2.5 Potentiodynamic Polarization Testing

The corrosion characteristics of CM-CoCr alloy and NT-DMLS-CoCr alloy specimens were examined by using potentiodynamic polarization testing in simulated body fluid (SBF). Before testing, the specimens were polished mechanically to a mirror finish, cleaned ultrasonically in ethanol, rinsed with distilled water, and dried. Electrochemical measurements were done with the help of a traditional three-electrode cell comprising of the Co-Cr specimen as the working electrode and a Saturated Calomel Electrode (SCE) as the reference electrode with a platinum electrode as the counter electrode [16]. The experiments were done at $37 \pm 1^{\circ}C$ to simulate physiological conditions. After stabilizing the open-circuit potential, polarization scans were conducted over a potential range of -1.0 V to +1.5 V with a scan rate of 1 mV/s. The corrosion potential (Ecorr), corrosion current density (Icorr), and corrosion rate were evaluated from the polarization curves by using Tafel extrapolation technique. Lower Icorr and corrosion rate values were noted as the indication of better corrosion resistance and passive film stability.

### 2.6 Bioactivity Evaluation

The bioactivity characteristics of CM-CoCr alloy and NT-DMLS-CoCr alloy specimens were examined with the help of immersion studies in Simulated Body Fluid (SBF) prepared as per Kokubo's protocol. The specimens were immersed in SBF at a physiological temperature of $37^{\circ}C$ for periods of 7, 14, 21, and 28 days to examine their capability to support apatite formation under situations similar to the human body environment [17]. The SBF solution was renewed once in every 48 hours to maintain the ionic concentration stable during the immersion time. After every immersion interval, the specimens were gently removed, rinsed with distilled water to remove loosely attached deposits, and dried at room temperature. The specimen's bioactivity was evaluated based on the amount of apatite layer formation and the capability of the implant surface to support biomineralization, which is a significant indicator of osseointegration potential in biomedical implant applications.

## 3 Results and Discussion

### 3.1 Wear Behavior Analysis

The wear characteristics of CM-CoCr alloy and NT-DMLS-CoCr alloy were examined under applied loads of 10 N, 30 N, and 50 N at a constant sliding velocity of 1.25 m/s and a sliding distance of 1000 m. The observed wear rate and coefficient of friction (CoF) values are given in Table 4.

**Table 4.** Wear Rate and Coefficient of Friction of CM-CoCr and NT-DMLS-CoCr

| Load (N) | Material | Wear Rate ($\times 10^{-5}$ mm$^3$/Nm) | COF |
|---|---|---|---|
| 10 | CM-CoCr | 1.82 | 0.41 |
| | NT-DMLS-CoCr | 1.12 | 0.32 |
| 30 | CM-CoCr | 3.76 | 0.48 |
| | NT-DMLS-CoCr | 2.08 | 0.37 |
| 50 | CM-CoCr | 6.24 | 0.55 |
| | NT-DMLS-CoCr | 3.46 | 0.43 |

It can be noted that there is a progressive increase in wear rate with an increase in applied load for both materials. This behavior is because of the increase in contact stress at the sliding interface, which induced the surface change, frictional heating, and material removal [18]. At an applied load of 10 N, the CM-CoCr specimen exhibited a wear rate of $1.82 \times 10^{-5}$ mm$^3$/Nm, whereas the NT-DMLS-CoCr specimen demonstrated a considerably lower wear rate of $1.12 \times 10^{-5}$ mm$^3$/Nm, corresponding to a reduction of approximately 38.5%. At 30 N, the wear rate decreased from $3.76 \times 10^{-5}$ mm$^3$/Nmfor CM-CoCr to $2.08 \times 10^{-5}$ mm$^3$/Nmfor NT-DMLS-CoCr, representing a reduction of approximately 44.7%. A similar trend was observed at the maximum applied load of 50 N, where the wear rates of CM-CoCr and NT-DMLS-CoCr were $6.24 \times 10^{-5}$ and $3.46 \times 10^{-5}$ mm$^3$/Nm, respectively. Thus, NT-DMLS-CoCr exhibited an approximately 44.6% reduction in wear rate compared with CM-CoCr under severe loading conditions.

The coefficient of friction also increased with increasing applied load for both specimens. The COF of CM-CoCr increased from 0.41 at 10 N to 0.55 at 50 N, whereas the corresponding values for NT-DMLS-CoCr increased from 0.32 to 0.43. At the maximum applied load, NT-DMLS-CoCr exhibited an approximately 21.8% lower COF than CM-CoCr. The lower friction coefficient indicates reduced resistance to sliding and improved tribological stability. The superior wear performance of NT-DMLS-CoCr can be attributed to the refined microstructure generated by rapid melting and solidification during DMLS

processing[19]. In addition, the optimized gyroid lattice architecture developed using nTopology software may facilitate more effective load distribution and reduce localized deformation, thereby minimizing material removal during sliding.

Figures 3(a) and 3(b) depict the SEM micrographs of the worn surfaces of CM-CoCr and NT-DMLS-CoCr specimens respectively examined at an applied load of 50 N. From Figure 3(a), it was noted that the worn surface of CM-CoCr shown relatively deep and continuous grooves over the sliding direction, along with extensive surface deformation, delaminated regions, and wear debris accumulation. The presence of pronounced grooves indicates severe abrasive wear caused by the repeated ploughing action of hard asperities and detached wear particles[20]. Localized material pull-out and delamination suggest that the increased contact stress at 50 N promoted subsurface deformation and the subsequent detachment of surface layers[21]. These surface features are consistent with the comparatively high wear rate and COF obtained for the CM-CoCr specimen.

In contrast, the SEM image of NT-DMLS-CoCr shown in Figure 3(b) exhibited comparatively shallow and narrow wear grooves, limited surface delamination, and reduced accumulation of wear debris. The smoother worn surface indicates reduced plastic deformation and improved resistance to material removal. The presence of fine grooves suggests that mild abrasive wear was the predominant wear mechanism. The refined DMLS microstructure and improved structural characteristics of the nTopology-designed specimen contributed to enhanced resistance against severe surface damage. The reduced degree of delamination and material pull-out observed on the NT-DMLS-CoCr surface supports the lower wear rate and coefficient of friction obtained experimentally.

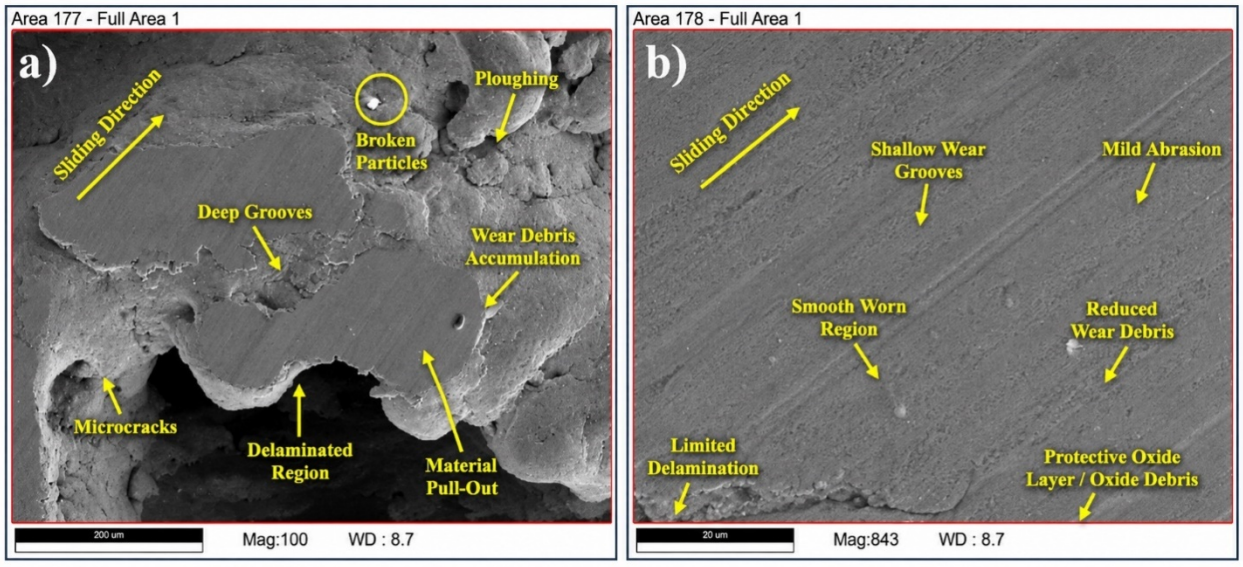



**Fig 3.** SEM micrographs of worn Co–Cr alloy surfaces after wear testing at 50 N: (a) CM-CoCr alloy and (b) NT-DMLS-CoCr alloy

Overall, the quantitative wear results and SEM observations confirm that NT-DMLS-CoCr possesses superior tribological performance compared with CM-CoCr. The observation of lesser wear rate, decreased friction coefficient, thin wear grooves, and minimal surface damage concludes the impact of nTopology-assisted DMLS fabrication for producing long-lasting Co-Cr components highly needed for load-bearing orthopedic and dental implant applications.

## 3.2 Potentiodynamic Polarization Behavior

The corrosion behavior of CM-CoCr alloy and NT-DMLS-CoCr alloy specimens was investigated using potentiodynamic polarization testing in simulated body fluid at physiological temperature. The corrosion parameters obtained from the polarization curves are presented in Table 5.

The potentiodynamic polarization curves of the CM-CoCr alloy and NT-DMLS-CoCr alloy specimens are presented in Figures 4(a) and 4(b), respectively. As observed from the polarization curves, both specimens exhibited active-to-passive electrochemical behavior in the simulated physiological environment, indicating the formation of a protective passive oxide film on the alloy surfaces. However, the polarization curve of NT-DMLS-CoCr was shifted toward a more positive potential and exhibited a lower corrosion current density than that of CM-CoCr. This shift indicates reduced electrochemical activity

**Table 5.** Potentiodynamic Polarization Results

| Material | Ecorr (mV) | Icorr ($\mu$A/cm$^2$) | Corrosion Rate (mm/year) |
|---|---|---|---|
| CM-CoCr | -352 | 1.76 | 0.017 |
| NT-DMLS-CoCr | -198 | 0.42 | 0.004 |

and improved resistance to anodic dissolution. The NT-DMLS-CoCr specimen exhibited a more positive corrosion potential (Ecorr) of -198 mV compared with -352 mV for CM-CoCr, indicating greater thermodynamic stability and a lower tendency toward corrosion initiation in SBF.

Furthermore, the corrosion current density (Icorr) decreased considerably from 1.76 $\mu$A/cm$^2$ for CM-CoCr to 0.42 $\mu$A/cm$^2$ for NT-DMLS-CoCr. This reduction corresponds to an improvement of approximately 76% in corrosion resistance. The lower current density observed in Figure 4(b) indicates a reduced rate of electrochemical dissolution and improved stability of the passive film formed on the NT-DMLS-CoCr surface. In contrast, the comparatively higher current density observed in Figure 4(a) indicates greater electrochemical activity and a higher rate of metallic dissolution in the conventionally manufactured specimen.

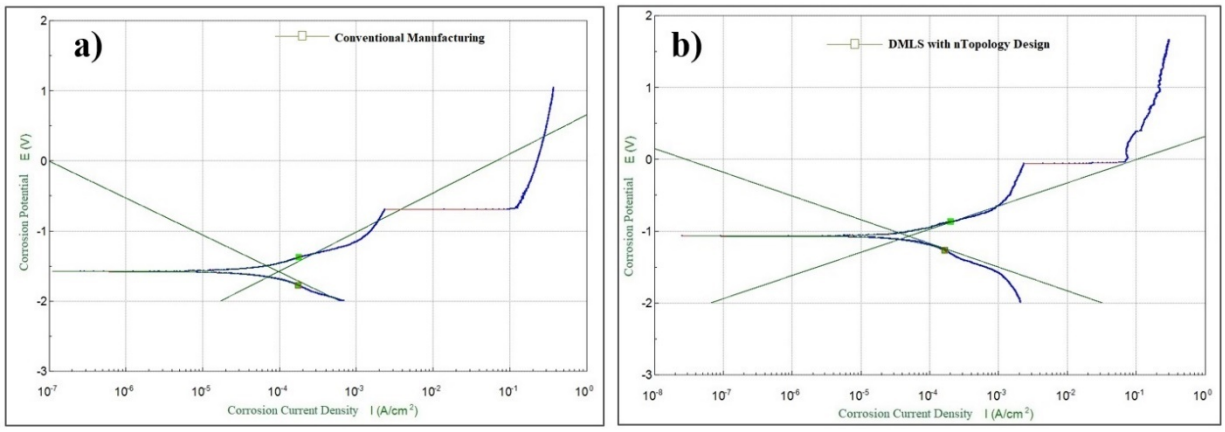



**Fig 4.** Potentiodynamic Polarization Curves of Co-Cr Alloys (a) Conventional Manufacturing (b) DMLS with nTopology Design

Similarly, the rate of corrosion got decreased from 0.017 mm/year for CM-CoCr to 0.004 mm/year for NT-DMLS-CoCr, representing a decrease of around 76.5%. The improved corrosion resistance of NT-DMLS-CoCr can be due to the development of a dense, uniform, and stable chromium-rich passive oxide layer over the DMLS-fabricated surface[22]. The quick melting and solidification resulted by DMLS process improve microstructural refinement and develop the homogeneity of the alloy, facilitating the formation of a more continuous protective passive layers. This stable oxide layer serves as a strong barrier between the metallic substrate and the simulated physiological environment, thereby reducing anodic dissolution and decreasing vulnerability to localized corrosion. The enhanced electrochemical stability of NT-DMLS-CoCr is beneficial for biomedical implant applications because it can reduce metallic ion release, protect structural integrity, and augment the long-term durability of implants under physiological conditions[23].

## 3.3 Bioactivity Performance

The bioactivity character of CM-CoCr and NT-DMLS-CoCr specimens was observed by immersion in simulated body fluid (SBF) for periods of 7, 14, 21, and 28 days. The level of apatite creation on the specimen surfaces was measured as relative apatite coverage and is depicted in Table 6.

The outcomes reveal that apatite formation is getting increased continuously with the increase in immersion duration for both the materials. However, NT-DMLS-CoCr constantly exhibited extensively better apatite coverage throughout the immersion period. After seven days of immersion, NT-DMLS-CoCr attained 24% apatite coverage, which was double than that of CM-CoCr (12%). Such tendency sustained throughout the experiment, with NT-DMLS-CoCr reaching 95% of surface coverage after twenty eight days compared with only 68% for CM-CoCr.

**Table 6.** Relative Apatite Coverage During SBF Immersion

| Immersion Period (Days) | CM-CoCr (%) | NT-DMLS-CoCr (%) |
|---|---|---|
| 7 | 12 | 24 |
| 14 | 28 | 52 |
| 21 | 48 | 76 |
| 28 | 68 | 95 |

The improved bioactivity of NT-DMLS-CoCr can be attributed to its interlinked lattice structure and increased surface area created by using nTopology design[24]. The porous pattern gives way to enhanced interaction between the SBF solution and implant surface, initiating adsorption of calcium and phosphate ions and stimulating apatite nucleation. Alternatively, the relatively dense structure of CM-CoCr offers few active nucleation sites, resulting in slow biomineralization. The quick formation of apatite on NT-DMLS-CoCr surfaces represents better osseointegration potential, which is important for achieving strong bone-implant bonding and for getting long-term implant success[25].

### 3.4 Comparative Performance Assessment

The combined results demonstrate that NT-DMLS-CoCr exhibited improved performance relative to CM-CoCr across all three investigated response categories. The maximum-load wear rate was reduced from $6.24 \times 10^{-5}$ to $3.46 \times 10^{-5}$ $mm^3/Nm$, corresponding to an approximately 44.6% reduction, while the COF decreased from 0.55 to 0.43. In electrochemical testing, the corrosion current density decreased from 1.76 to 0.42 $\mu A/cm^2$ and the corrosion rate decreased from 0.017 to 0.004 mm/year. Bioactivity evaluation further demonstrated that apatite coverage increased from 68% for CM-CoCr to 95% for NT-DMLS-CoCr after 28 days of SBF immersion.

Overall, the results indicate that the combination of nTopology-based gyroid lattice design and DMLS fabrication can provide a favorable balance of tribological performance, electrochemical stability, and in-vitro bioactive response compared with conventionally manufactured Co–Cr under the conditions investigated. The findings support the potential of NT-DMLS-CoCr as an architecturally engineered Co–Cr material for biomedical implant applications, while further fatigue, tribocorrosion, cytocompatibility, and in-vivo investigations are required before broader clinical conclusions can be established.

## 4 Conclusion

The present study comparatively investigated the wear behavior, potentiodynamic polarization behavior, and bioactivity performance of CM-CoCr and NT-DMLS-CoCr for biomedical implant applications. The results demonstrated that the manufacturing route and internal architectural design significantly influenced the functional performance of the Co–Cr alloy under the investigated experimental conditions.

The wear results showed that the wear rate increased with increasing applied load for both materials. However, NT-DMLS-CoCr consistently exhibited lower wear rates and coefficients of friction than CM-CoCr at all investigated loads. At the maximum applied load of 50 N, the wear rate of NT-DMLS-CoCr was $3.46 \times 10^{-5}$ $mm^3/Nm$, compared with $6.24 \times 10^{-5}$ $mm^3/Nm$ for CM-CoCr, representing an approximately 44.6% reduction. The improved tribological response of NT-DMLS-CoCr was associated with the DMLS-fabricated material condition and the selected interconnected gyroid architecture, which contributed to improved resistance against surface damage under the investigated sliding conditions.

The potentiodynamic polarization results demonstrated superior electrochemical performance for NT-DMLS-CoCr. The corrosion current density decreased from 1.76 $\mu A/cm^2$ for CM-CoCr to 0.42 $\mu A/cm^2$ for NT-DMLS-CoCr, corresponding to an approximately 76% reduction. Similarly, the corrosion rate decreased from 0.017 to 0.004 mm/year. The more positive corrosion potential and lower corrosion current density indicate improved electrochemical stability of NT-DMLS-CoCr in the simulated physiological environment. The improved response may be associated with the formation and stability of the protective chromium-rich passive film; however, direct characterization of the passive layer was not performed in the present study.

The bioactivity results demonstrated progressively increasing apatite formation with increasing SBF immersion duration for both materials, with NT-DMLS-CoCr consistently exhibiting higher apatite coverage. After 28 days, NT-DMLS-CoCr achieved approximately 95% apatite coverage, compared with 68% for CM-CoCr. The enhanced apatite formation can be reasonably associated with the interconnected gyroid architecture and its increased accessible surface area, which can promote interaction between the material and simulated physiological environment.

Overall, NT-DMLS-CoCr exhibited improved wear resistance, electrochemical corrosion resistance, and in-vitro bioactive response compared with CM-CoCr under the conditions investigated. The principal contribution of the study is the integrated comparison of a computationally designed gyroid architecture fabricated by DMLS with conventionally manufactured Co–Cr using three complementary biomedical performance characteristics. These findings indicate the potential of nTopology-assisted DMLS fabrication for architecturally engineered Co–Cr implants. However, further investigations involving tribocorrosion, fatigue behavior, cytocompatibility, long-term degradation, and in-vivo studies are required to establish the long-term biological and mechanical suitability of the proposed implant structure.

## 5 Acknowledgements

Nil

*Author details*: Rajitha N is a Research Scholar, Srinivasan V is an Associate Professor; Sathishkumar G B is an Assistant Professor.

## References

1) Hrir H, Boudouma A, Layachi OA, Harrati A, Hsissou R, Khoumri E. An in-depth review of corrosion pathways in titanium dental and orthopedic implants and their biological interactions. *Biomedical Materials & Devices*. 2026;4(1):446–466. https://doi.org/10.1007/s44174-025-00300-w.
2) Tripathi S, Raheem A, Dash M, Kumar P, Elsebahy A, Singh H, et al. Surface engineering of orthopedic implants for better clinical adoption. *Journal of Materials Chemistry B*. 2024;12(44):11302–11335. https://doi.org/10.1039/d4tb01563k.
3) Hashemi N, Yahyavi S, Bakhshayesh MM, Khodabakhshi F, Aghdam RM. Bio-tribo-corrosion behavior of additively manufactured Co-Cr dental implant alloy. *Surface and Coatings Technology*. 2025;512:132422. https://doi.org/10.1016/j.surfcoat.2025.132422.
4) Makuochukwu OT, Ilemona AE. Titanium, Stainless Steel and Cobalt-chromium-based Alloys: Classification and Diverse Applications. *International Journal of Materials Science*. 2026;15(3):100–112. https://doi.org/10.11648/j.ijmsa.20261503.13.
5) Nouri A, Shirvan AR, Li Y, Wen C. Surface modification of additively manufactured metallic biomaterials with active antipathogenic properties. *Smart Materials in Manufacturing*. 2023;1:100001. https://doi.org/10.1016/j.smmf.2022.100001.
6) Tabrizian P, Davis S, Su B. From bone to nacre–development of biomimetic materials for bone implants: a review. *Biomaterials Science*. 2024;12(22):5680–5703. https://doi.org/10.1039/d4bm00903g.
7) Kelvin-Agwu MC, Adelodun MO, Igwama GT, Anyanwu EC. Advancements in biomedical device implants: A comprehensive review of current technologies. *International Journal of Frontiers in Medical and Surgical Research*. 2024;6(01):19–28. https://doi.org/10.53294/ijfmsr.2024.6.1.0037.
8) Said LB, Ayadi B, Alharbi S, Dammak F. Recent advances in additive manufacturing: a review of current developments and future directions. *Machines*. 2025;13(9):813. https://doi.org/10.3390/machines13090813.
9) Boretti A. Metal additive manufacturing for internal combustion engine components: A narrative review of applications, materials, processes, challenges, and future directions. *The International Journal of Advanced Manufacturing Technology*. 2025;139(11):6355–6397. https://doi.org/10.1007/s00170-025-16219-x.
10) Siddiqui MA, Mia MP, Hossain MA, Rabbi MS, Butt H, Alam F. Recent Advances in Crystalline Architecture and Defect Engineering of 3D-Printed Metals for Biomedical Breakthroughs: A Comprehensive Review. *Advanced Engineering Materials*. 2025;27(16):2500257. https://doi.org/10.1002/adem.202500257.
11) Liu F, Shao Y, Chen M. Generative design strategies for additive manufacturing of lattice structures: A review. *Materials & Design*. 2026;2:115431. https://doi.org/10.1016/j.matdes.2026.115431.
12) Khan N, Riccio A. A systematic review of design for additive manufacturing of aerospace lattice structures: Current trends and future directions. *Progress in Aerospace Sciences*. 2024;149:101021. https://doi.org/10.1016/j.paerosci.2024.101021.
13) Sathishkumar GB, Asaithambi B, Srinivasan V, Karthikeyan T. Laser Cladding of AZ61 Magnesium Alloy Reinforced with Inconel 625 Particle: A Grey Relational Analysis Approach. *Materials Research*. 2025;28:e20250352. https://doi.org/10.1590/1980-5373-MR-2025-0352.
14) Sathishkumar GB, Asaithambi B, Srinivasan V. Optimizing laser cladding parameters on AZ61 magnesium alloy with inconel 625 powder through grey relation analysis. *Indian Journal of Science and Technology*. 2024;17(11):1059–1069. https://doi.org/10.17485/IJST/v17i11.2686.
15) Sathishkumar GB, Asaithambi B, Srinivasan V. Surface modification of AZ61 magnesium alloy with stelcar alloy powder using laser cladding technique. *Indian Journal of Science and Technology*. 2024;17(14):1485–1496. https://doi.org/10.17485/IJST/v17i14.187.
16) Reclaru L, Buciu G, Petrescu SM, Gheorghe RI, Grecu DF, Grecu AF. Corrosion Behavior and Ion Release of Co–Cr Dental Alloys Fabricated by Casting, CAD/CAM, SLM and DMLS: Influence of Manufacturing Route and Microstructure. *Bioengineering*. 2026;13(4):406. https://doi.org/10.3390/bioengineering13040406.
17) Joseph A, Uthirapathy V. A systematic review of the contribution of additive manufacturing toward orthopedic applications. *ACS Omega*. 2024;9(44):44042–44075. https://doi.org/10.1021/acsomega.4c04870.
18) Schwindling FS, Seubert M, Rues S, Koke U, Schmitter M, Stober T. Two-body wear of CoCr fabricated by selective laser melting compared with different dental alloys. *Tribology Letters*. 2015;60(2):25. https://doi.org/10.1007/s11249-015-0601-7.
19) Fellah M, Hezil N, Bouras D, Obrosov A, Mohammed AS, Montagne A, et al. Structural, mechanical and tribological performance of a nano structured biomaterial Co–Cr–Mo alloy synthesized via mechanical alloying. *Journal of Materials Research and Technology*. 2023;25:2152–2165. https://doi.org/10.1016/j.jmrt.2023.06.031.
20) Wang C, Lu X, Yang X, Zuo H, Li MV, Zhao X, et al. Biomimetic Kagome-Gyroid interpenetrating metamaterial for tailoring lightweight and mechanical performance. *Materials & Design*. 2025;252:113729. https://doi.org/10.1016/j.matdes.2025.113729.
21) Bonilauri MF, Perini M, Amirabdollahian S, Paglia L, Pulci G, Marra F, et al. Deposition of high-velocity oxygen-fuel (HVOF) coatings on laser-powder bed fused (L-PBF) parts subjected to in-situ laser remelting treatments. *Surface and Coatings Technology*. 2025;510:132250. https://doi.org/10.1016/j.surfcoat.2025.132250.

22) Zhao W, Cai DJ, Wu X, Liu YJ, Xu P, Gao YH, et al. Upgrading mechanical property and corrosion resistance of a low cost 45 steel by remelting a Cr film of $\sim$1 $\mu$m in thickness. *Journal of Materials Research and Technology*. 2023;26:8961–8971. https://doi.org/10.1016/j.jmrt.2023.09.221.
23) Ghoncheh MH, Shahriari A, Birbilis N, Mohammadi M. Process-microstructure-corrosion of additively manufactured steels: a review. *Critical Reviews in Solid State and Materials Sciences*. 2024;49(4):607–717. https://doi.org/10.1080/10408436.2023.2255616.
24) Tuninetti V, Narayan S, Ríos I, Menacer B, Valle R, Al-Lehaibi M, et al. Biomimetic lattice structures design and manufacturing for high stress, deformation, and energy absorption performance. *Biomimetics*. 2025;10(7):458. https://doi.org/10.3390/biomimetics10070458.
25) Li J, Fan H, Li H, Hua L, Du J, He Y, et al. Recent advancements in the surface modification of additively manufactured metallic bone implants. *Additive Manufacturing Frontiers*. 2025;4(1):200195. https://doi.org/10.1016/j.amf.2025.200195.